JPEDAV (2015) 36:224–240
DOI: 10.1007/s11669-015-0376-4
1547-7037 ©ASM International

Critical Assessment and Thermodynamic Modeling of the Fe-O-S System

Denis Shishin, Evgueni Jak, and Sergei A. Decterov

(Submitted December 23, 2014; in revised form February 13, 2015; published online March 13, 2015)

The Fe-O-S system has been assessed over the whole composition range to produce a self-consistent set of thermodynamic properties of all condensed phases from 298 K to above the liquidus temperatures at ambient pressure. The liquid phase from metallic liquid to sulfide melt to oxide melt is described by a single model developed within the framework of the quasi-chemical formalism. The model reflects the existence of strong short-range ordering in oxide, sulfide and oxysulfide liquid. Two ranges of maximum short-range ordering in the Fe-O system at approximately FeO and Fe_2O_3 compositions are taken into account. Parameters of thermodynamic models have been optimized to reproduce all available thermodynamic and phase equilibrium data. The thermodynamic modeling of the Fe-O-S system performed in the present study is of particular importance for the description of the solubility of oxygen in matte.

Keywords CALPHAD approach, critical assessment, liquidus, optimization, phase diagram, thermodynamic modeling, thermodynamic properties

1. Introduction

The present study is part of an ongoing research project which is aimed at developing a thermodynamic database for simulation of copper extraction from sulfide concentrates. The previous article dealt with the Cu-O-S system.[1] The major phases that form during copper smelting and converting are: blister copper (a liquid metal phase rich in Cu), matte (a molten sulfide phase containing mainly Cu, S and Fe), slag (a molten oxide phase) and gas. In principle, all three liquid phases represent just one liquid with miscibility gaps. Liquid metal, matte and slag can be completely miscible over certain ranges of temperature and composition, even though this normally does not happen under industrial conditions. It is desirable to have one general thermodynamic model which can describe all three liquid phases simultaneously, but this is very difficult to achieve because the model must reflect quite different atomic interactions that are intrinsic to metallic, sulfide and oxide phases.

Denis Shishin, Centre de Recherche en Calcul Thermochimique (CRCT), Deép. de Geénie Chimique, É cole Polytechnique, Montreal, QC, Canada; **Evgueni Jak**, PYROSERCH (Pyrometallurgy Research), School of Engineering, The University of Queensland, Brisbane, QLD, Australia; and **Sergei A. Decterov**, Centre de Recherche en Calcul Thermochimique (CRCT), Deép. de Geénie Chimique, Eé cole Polytechnique, Montreal, QC, Canada and PYROSERCH (Pyrometallurgy Research), School of Engineering, The University of Queensland, Brisbane, QLD, Australia.Contact e-mails: d.shishin@uq.edu.au,e.jak@uq.edu.au, and sergei.decterov@polymtl.ca

As in the case of slags, mattes exhibit strong first-nearest-neighbor (FNN) short-range ordering (SRO). Metal-sulfur pairs in matte are energetically favored over metal-metal and sulfur-sulfur pairs, but contrary to oxide melts, such as CaO-SiO_2, where the ratio O/(Ca + 2Si) is always very close to 1, the composition of matte can substantially deviate from stoichiometric sulfides both towards metals and nonmetals. In the Fe-S system there is even no miscibility gap between liquid metal and liquid sulfide.

This study presents the thermodynamic modeling and optimization of model parameters for the Fe-O-S system, which complete "optimization" of all binary and ternary subsystems of the Cu-Fe-O-S system using the Calphad technique. The results of the present study can be combined with the optimizations of the Cu-Fe-S,[2–4] Cu-O-S,[1] Fe-O[5] and Cu-Fe-O[6] systems to predict thermodynamic properties and phase equilibria in the Cu-Fe-O-S quaternary system. Comparison of these predictions with the available experimental data will be reported elsewhere.

In the present study, all calculations were carried out using the FactSage thermochemical software and databases.[7]

2. Thermodynamic Models

The models for the liquid phase, monoxide, bcc and fcc solid solutions are discussed below. The models for spinel (magnetite) and pyrrhotite ($Fe_{1-x}S$) were reported earlier.[2,8]

2.1 Liquid Solution

No attempts were found in the literature to model the liquid phase in the Fe-O-S system over the entire composition range from liquid metal to oxysulfide melt. The thermodynamic model must describe drastic changes in the activities of sulfur and oxygen which are the result of strong SRO at the FeS and FeO compositions, respectively. Furthermore, in the Fe-O system, a second maximum in SRO is to be expected at the Fe_2O_3 composition, even

though no experimental data are available in this region because of very high equilibrium oxygen pressures.

Thermodynamic modeling of the liquid phase and the available experimental data for the Fe-O and Fe-S systems were reviewed by Hidayat et al.[5] and Waldner and Pelton,[2] respectively.

In the present study, a model for the liquid phase is developed within the framework of the quasichemical formalism.[9,10] It has one sublattice containing four species: Fe^{II}, Fe^{III}, S and O, where Fe^{II} and Fe^{III} correspond to two oxidation states of Fe. In the Fe-O system, the fraction of the Fe^{II}-O pairs goes through a maximum close to the FeO composition, while the Fe^{III}-O pairs are most abundant at the Fe_2O_3 composition. All species are not charged, so the condition of electroneutrality is not imposed and the model is capable to represent the liquid phase from metal to nonmetals.

The formulae and notations of the quasichemical formalism have been described in detail elsewhere[9,10] and only a brief summary is given here. To explain the meaning of parameters of the quasichemical formalism, let us consider a binary solution formed by components A and B. In the pair approximation of the modified quasichemical model, the following pair exchange reaction is considered:

$$(\text{A-A}) + (\text{B-B}) = 2(\text{A-B});\ \Delta g_{\text{AB}} \qquad \text{(Eq 1)}$$

where (i–j) represents a FNN pair and Δg_{AB} is the non-configurational Gibbs energy change for the formation of two moles of (A-B) pairs.

When the solution is formed from pure components A and B, some (A-A) and (B-B) pairs break to form (A-B) pairs, so the Gibbs energy of mixing is given by[9]:

$$\Delta G_{\text{mix}} = G - (n_{\text{A}} g_{\text{A}}^{\circ} + n_{\text{B}} g_{\text{B}}^{\circ}) = -T\Delta S^{\text{config}} + \left(\frac{n_{\text{AB}}}{2}\right)\Delta g_{\text{AB}} \qquad \text{(Eq 2)}$$

where G is the Gibbs energy of the solution, g_{A}° and g_{B}° are the molar Gibbs energies of pure liquid components; n_{A}, n_{B} and n_{AB} are the numbers of moles of A, B and (A-B) pairs and ΔS^{config} is the configurational entropy given by randomly mixing the (A-A), (B-B) and (A-B) pairs. Since no exact expression is known for this entropy of mixing in three dimensions, an approximate equation is used which was shown[9] to be an exact expression for a one dimensional lattice (Ising model) and to correctly reduce to the random mixing point approximation (Bragg Williams model) when Δg_{AB} is equal to zero.

Δg_{AB} can be expanded as an empirical polynomial in terms of the mole fractions of pairs[9]:

$$\Delta g_{\text{AB}} = \Delta g_{\text{AB}}^{\circ} + \sum_{(i+j)\geq 1} g_{\text{AB}}^{ij} X_{\text{AA}}^{i} X_{\text{BB}}^{j} \qquad \text{(Eq 3)}$$

where $\Delta g_{\text{AB}}^{\circ}$ and g_{AB}^{ij} are the parameters of the model which can be functions of temperature. In practice, only the parameters g_{AB}^{i0} and g_{AB}^{0j} need to be included.

The composition of maximum SRO is determined by the ratio of coordination numbers. Let Z_{A} and Z_{B} be the coordination numbers of A and B. These coordination numbers can vary with composition as follows[9]:

$$\frac{1}{Z_{\text{A}}} = \frac{1}{Z_{\text{AA}}^{\text{A}}}\left(\frac{2n_{\text{AA}}}{2n_{\text{AA}} + n_{\text{AB}}}\right) + \frac{1}{Z_{\text{AB}}^{\text{A}}}\left(\frac{n_{\text{AB}}}{2n_{\text{AA}} + n_{\text{AB}}}\right) \qquad \text{(Eq 4)}$$

$$\frac{1}{Z_{\text{B}}} = \frac{1}{Z_{\text{BB}}^{\text{B}}}\left(\frac{2n_{\text{BB}}}{2n_{\text{BB}} + n_{\text{AB}}}\right) + \frac{1}{Z_{\text{BA}}^{\text{B}}}\left(\frac{n_{\text{AB}}}{2n_{\text{BB}} + n_{\text{AB}}}\right) \qquad \text{(Eq 5)}$$

where Z_{AA}^{A} and Z_{AB}^{A} are the values of Z_{A} when all nearest neighbors of an A are As, and when all nearest neighbors of an A are Bs, respectively, and where Z_{BB}^{B} and Z_{BA}^{B} are defined similarly. For example, in order to set the composition of maximum SRO at the molar ratio $n_{\text{A}}/n_{\text{B}} = 2$, one can set the ratio $Z_{\text{BA}}^{\text{B}}/Z_{\text{AB}}^{\text{A}} = 2$. Values of Z_{BA}^{B} and Z_{AB}^{A} are unique to the A-B binary system, while the value of Z_{AA}^{A} is common to all systems containing A as a component.

Even though the model is sensitive to the ratio of the coordination numbers, it is less sensitive to their absolute values. We have found by experience that selecting values of the coordination numbers that are smaller than actual values often yields better results. This is due to the inaccuracy introduced by an approximate equation for the configurational entropy of mixing which is only exact for a one dimensional lattice. The smaller coordination numbers partially compensate this inaccuracy in the model equations, being more consistent with a one dimensional lattice. Therefore, the "coordination numbers" in our model are essentially treated as model parameters which are used mainly to set a physically reasonable composition of maximum SRO.

There are ten possible pairs formed by the species Fe^{II}, Fe^{III}, O and S in the Fe-O-S liquid phase. The fractions of all pairs are calculated by the Gibbs energy minimization procedure built into the FactSage software[7] using the optimized model parameters. Fe^{II}-Fe^{II}, O-O and S-S are the predominant pairs at compositions close to pure Fe, O and S, respectively. The Fe^{II}-O, Fe^{III}-O and Fe^{II}-S pairs are dominant in the oxide and sulfide liquids, whereas the fractions of the Fe^{II}-Fe^{III}, Fe^{III}-Fe^{III}, O-S and Fe^{III}-S pairs are small at all compositions of interest.

"Coordination-equivalent" fractions (Y_{m}) are defined as

$$Y_{\text{m}} = Z_{\text{m}} n_{\text{m}} / \sum (Z_i n_i) \qquad \text{(Eq 6)}$$

In addition to the binary terms, the model can have ternary terms, $\Delta g_{\text{AB(C)}}$, which give the effect of the presence of component C upon the energy Δg_{AB} of pair exchange reaction (1). Ternary terms are expanded as empirical polynomials either in terms of the mole fractions of pairs (with model parameters $g_{\text{AB(C)}}^{ijk}$) or in terms of the "coordination-equivalent" fractions (with model parameters $q_{\text{AB(C)}}^{ijk}$). In the quasichemical formalism, it is also possible to have Bragg Williams ternary terms, which are essentially the same as $q_{\text{AB(C)}}^{ijk}$ terms, except for they are not taken into account in the calculation of the amounts of pairs.

Extrapolation of binary terms into the Fe^{II}-Fe^{III}-O-S system is done by an asymmetric "Toop-like" method.[10] The components are divided into two groups: metals (Fe^{II}

and Fe^{III}) and nonmetals (S and O). By this means in every ternary subsystem, one component belongs to a different group than the other two. "Toop-like" extrapolation is applied, taking this "different" component as an asymmetric component. The formulae for ternary terms and for extrapolation of binary and ternary terms into a multicomponent system are discussed in detail elsewhere.[10]

2.2 Solid FCC and BCC Iron

Sulfur and oxygen are soluble to some extent in Fe metal, which has an fcc or bcc structure at the conditions of interest. The Bragg-Williams random mixing model was used for both phases with the following formula (per mole of atoms):

$$g = (X_{Fe}g^{o}_{Fe} + X_{O}g^{o}_{O} + X_{S}g^{o}_{S}) + RT(X_{Fe}\ln X_{Fe} + X_{O}\ln X_{O} + X_{S}\ln X_{S}) + X_{Fe}X_{S}L_{Fe,S} + X_{Fe}X_{O}L_{Fe,O} \quad \text{(Eq 7)}$$

where X_i and g°_{i} are the mole fraction and molar Gibbs energy of component i, $L_{i,j}$ represents the interaction energy between i and j, which can be a function of temperature and composition.

2.3 Monoxide (wüstite)

Vogel and Fulling[11] carried out equilibration and quenching experiments followed by analysis and reported that FeO and FeS are immiscible. Johto et al.[12] also reported that sulfur was not soluble in wüstite based on equilibration/quenching/EMPA experiments. Hence, sulfur was assumed to be insoluble in monoxide.

The simplest polynomial model that was used for wüstite in the Fe-O system[5] is accepted in the present study. It describes the nonstoichiometry of the wüstite phase towards oxygen using the Bragg-Williams approximation and assuming random mixing of Fe^{2+} and Fe^{3+} ions on cation sites. This assumption does not correspond to the real structure of wüstite, which is rather complex and not completely understood. However, it was shown in the assessment of the Fe-O system[5] that different models give almost identical representations of the entropy of wüstite as a function of composition, provided that the models adequately reproduce the absolute entropies of wüstite at several compositions and 25 °C, which were obtained by the integration of the experimental low-temperature heat capacities.

The Gibbs energy per mole of components FeO and $FeO_{1.5}$ is given by

$$g = (X_{FeO}g^{o}_{FeO} + X_{FeO_{1.5}}g^{o}_{FeO_{1.5}}) + RT(X_{FeO}\ln X_{FeO} + X_{FeO_{1.5}}\ln X_{FeO_{1.5}}) + X_{FeO}X_{FeO_{1.5}}L_{FeO,FeO_{1.5}} \quad \text{(Eq 8)}$$

where g^{o}_{M} and X_M are the Gibbs energy and mole fraction of pure component M, respectively. The molar interaction energy $L_{M,N}$ between components M and N is expanded as a polynomial in the mole fractions of the components:

$$L_{M,N} = \sum_{i,j\geq 0} q^{ij}_{M,N}X^{i}_{M}X^{j}_{N} \quad \text{(Eq 9)}$$

where $q^{ij}_{M,N}$ are the binary model parameters.

3. The Fe-S System

The Fe-S system was optimized by Waldner and Pelton.[2] The phase diagram is shown in Fig. 1. Comparisons with the experimental data, descriptions of thermodynamic models and optimized model parameters for all phases are given in Ref 2. The description of the Fe-S liquid phase optimized by Waldner and Pelton[2] was accepted in the present study with minor modifications. Contrary to the Fe-O liquid, the Fe-S liquid phase was modeled in such a way that Fe exists almost exclusively as Fe^{II} over the whole composition range from metal to sulfur. This is because solid Fe_2S_3 is not stable and there is no experimental evidence for strong SRO in the liquid phase at the Fe_2S_3 composition which corresponds to very high S_2 partial pressures.

A small modification of the $\Delta g^{\circ}_{Fe^{II}S}$ parameter for the liquid phase was made in the present study to improve the description in the liquid iron region at 1500-1600 °C. The resulted changes in the description of the system below 1500 °C are minimal compared to the original study of Waldner and Pelton.[2] Even though some of the experimental data in the temperature range of 1600-1730 °C seem to be fitted not as good as by Waldner and Pelton,[2] the region from 1500 to 1600 °C is more important for industrial applications and the experimental measurements are more accurate there. The differences are discussed in more detail elsewhere.[13]

4. The Fe-O System

The Fe-O system was reevaluated recently[5] and the optimized phase diagram is shown in Fig. 2.

5. The Fe-O-S System

5.1 Phase diagrams

There are two ternary compounds in the Fe-O-S system, $FeSO_4$ and $Fe_2(SO_4)_3$, which decompose forming the gas phase before melting at ambient pressure. Subsolidus reactions were studied by Skeaf and Espelund,[14] Hsieh and Chang,[15] Rosenqvist and Hofseth,[16] Musbah and Chang,[17] Schaefer[18] and Espelund and Jynge[19] using the EMF technique in flowing SO_2. Their data are summarized in Fig. 3. Most likely, these experiments do not correspond to equilibrium with the gas phase, which can contain other gaseous species such as SO_3, S_2 and O_2, but rather to a fixed potential of SO_2, i.e. the other gaseous species do not form

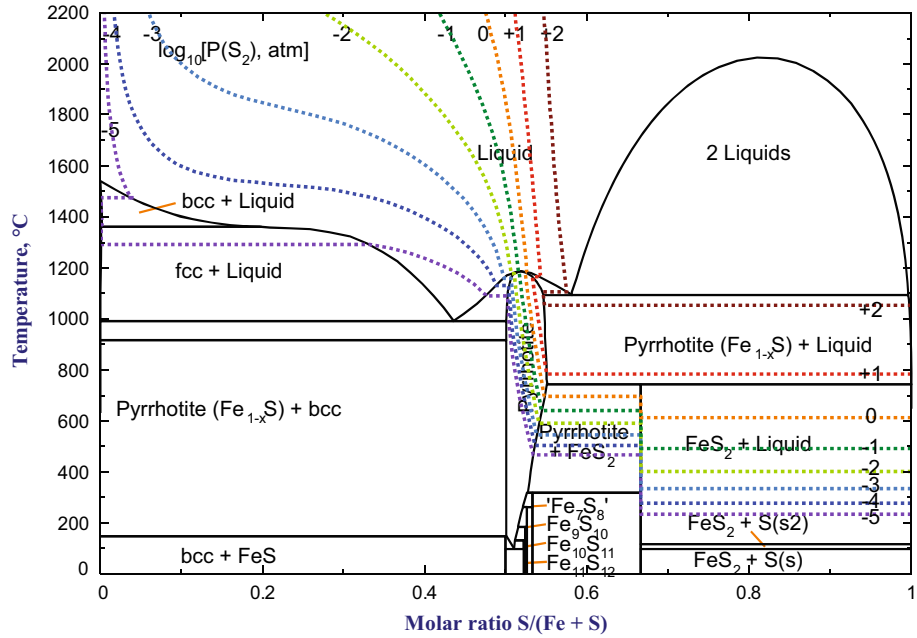

Fig. 1 Calculated phase diagram of the Fe-S system with superimposed S_2 isobars. Formation of the gas phase is suppressed

fast enough to significantly change the composition of flowing SO_2. If the equilibrium with the gas phase were attained, it would be almost pure SO_2 over the range of $P(O_2)$ from 10^{-4} to 10^{-14} atm. At higher oxygen potentials, amounts of SO_3 and O_2 become substantial, while at lower $P(O_2)$ the partial pressure of S_2 starts to increase. The composition of the gas flowing out of the furnace was not analyzed, but our calculations showed that large amounts of condensed phases in EMF cells would have to react in order to produce the gas phase of equilibrium composition, which is not what happened in the experiments.

Rosenqvist and Hynne[20] carried out equilibration, quenching and analysis experiments and reported that FeS does not dissolve in Fe_3O_4 spinel.

Liquid that appears in the system expands from molten nonstoichiometric FeS towards FeO. At high temperatures it also spreads to liquid metal. The evaluated phase diagram of the Fe-O-S system at 1200 °C and at the total pressure of 1 atm is shown in Fig. 4.

Phase equilibria in the Fe-S-O system were studied repeatedly.[11,12,21–29]

Naldrett[25] determined the iron-wüstite-troilite-liquid (Fe-"FeO"-"FeS"-L) ternary eutectic temperature by melting pyrrhotite, wüstite and iron in silica, iron or silver crucibles. Experiments in silica and iron crucibles gave 915 ± 2 °C, while in silver crucibles the eutectic temperature was measured to be 905 ± 2 °C. The composition of this eutectic was determined by melting in silver crucibles and is shown in Fig. 5. Even though the eutectic temperature obtained in silver crucibles was lower, the author claimed that the presence of Ag had only a small effect on the Fe:S:O ratio in the liquid phase at the eutectic temperature. Naldrett[25] also reported the temperature and composition of the magnetite-wüstite-troilite-liquid ("Fe_3O_4"-"FeO"-"FeS"-L) ternary peritectic. The experiments were conducted in evacuated and sealed silica tubes, hence it was possible to study melts with high equilibrium vapor pressures without affecting the composition. The results obtained in contact with silica tubes should probably be interpreted as corresponding to the Fe-O-S-Si system at SiO_2 saturation. Naldrett suggested that since the presence of SiO_2 did not affect much the temperature of the Fe-"FeO"-"FeS"-L eutectic, it should not have a strong effect on the "Fe_3O_4"-"FeO"-"FeS"-L invariant temperature and composition. The temperature was found to be 934 ± 2°C and the composition is shown in Fig. 5.

The experiments of Hilty and Crafts[21] involved melting mixtures of FeS and Fe_2O_3 in iron crucibles. The melting was carried out in Ar, assuming that the O:S ratio in the samples did not change significantly due to low $P(SO_2)$ and $P(S_2)$ in the iron-saturated system. Taking into account the fluctuations of cool Ar flow, the accuracy in temperature determination suggested by the authors was ±10 °C. Preliminary studies were conducted to prove that the reaction time of 2 h was sufficient for equilibration. After equilibration, samples were quenched in water and studied by chemical analysis and microscopic examination. The results are plotted in Fig. 5 and 6(a-f).

Darken and Gurry (cited in Ref 22) melted the charge of pyrrhotite and wüstite. The composition of pyrrhotite corresponded to $FeS_{0.942}$ and that of wüstite—to $FeO_{1.054}$. Samples were placed in iron crucibles in an atmosphere of purified N_2 and annealed at controlled temperature. No special precautions were made in order to keep the samples on the $FeS_{0.942}$-$FeO_{1.054}$ section, so the initial compositions could have changed due to dissolution of iron from the crucibles or evaporation of oxygen and sulfur into the gas

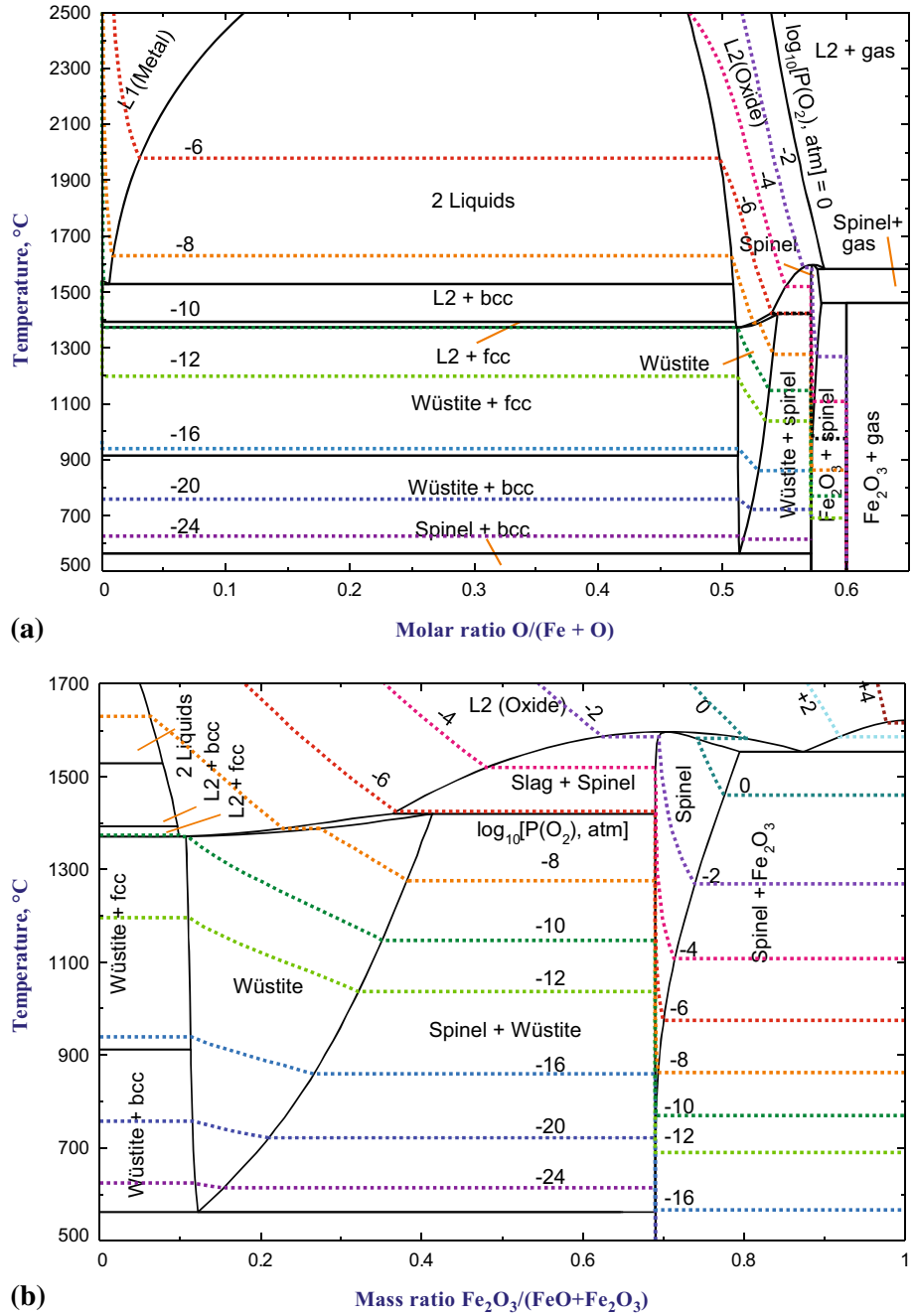

Fig. 2 (a) Optimized phase diagram of the Fe-O system.[5] The dashed lines are calculated oxygen isobars. The gas phase is suppressed. (b) Enlarged FeO-Fe_2O_3 part of the same diagram

phase. The phase boundaries corresponding to precipitation of the pyrrhotite and wüstite phases were obtained by microscopic examination of samples quenched into mercury. The structural characteristics of the polished samples made it possible to determine whether quenching was made from the temperatures above or below these phase boundaries. The compositions of the liquid phase were not measured, which increases the uncertainty of the determined phase boundaries. These experimental points are plotted in Fig. 7, assuming that the samples were in equilibrium with iron and that the O:S ratio in the samples did not change during the experiments.

Vogel and Fulling[11] used corundum crucibles to melt mixtures of Fe, Fe_2O_3 and S in Ar. Quenched samples were examined microscopically. The temperature of 920 °C was measured for the Fe-"FeS"-"FeO"-L eutec-

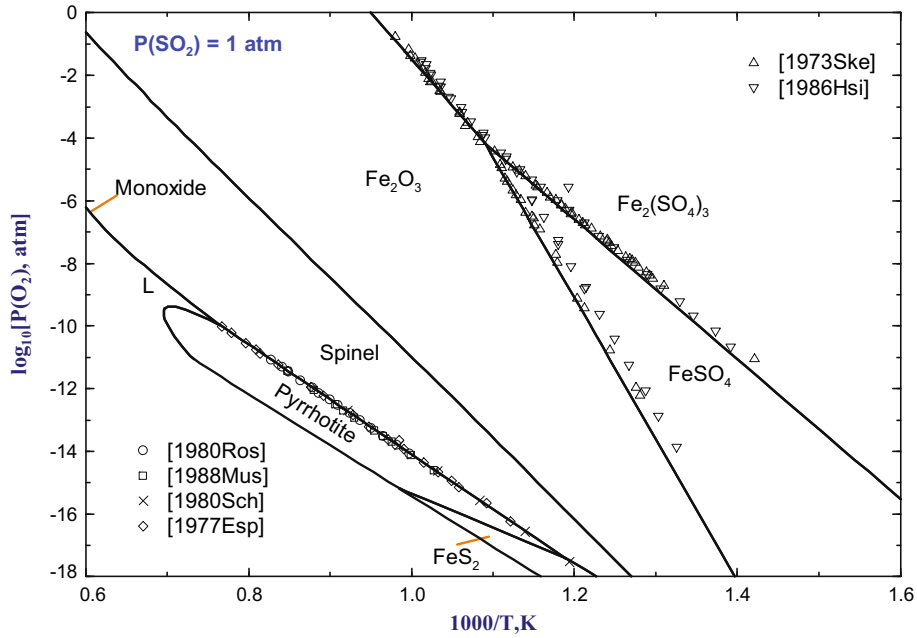

Fig. 3 Potential phase diagram of the Fe-O-S system at $P(SO_2)$ = 1 atm

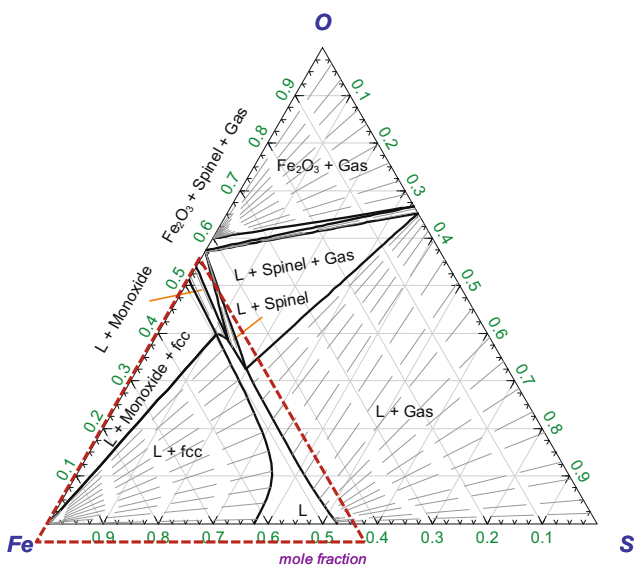

Fig. 4 Calculated isothermal section of the Fe-O-S phase diagram at 1200 °C and P = 1 atm

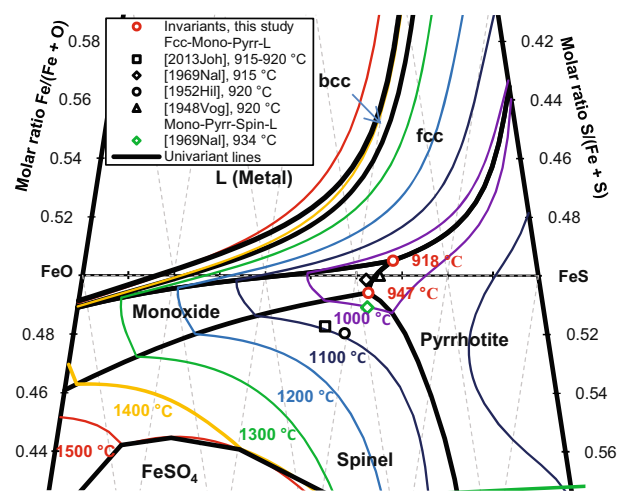

Fig. 5 Liquidus projection of the Fe-O-S system (FeO-FeS region). Formation of the gas phase is suppressed. Points show the compositions of invariant points reported in studies[11,12,21,25]

tic. The composition of this eutectic is shown in Fig. 5. The authors also reported the "FeO-FeS" section of the Fe-O-S phase diagram, but it remains unclear how much the actual compositions of their samples deviated from this section. As can be seen from Fig. 5, iron must have precipitated from the initial compositions along most of the FeO-FeS section to produce oxysulfide liquid in equilibrium with monoxide (wüstite). Hence, the monoxide liquidus reported by Vogel and Fulling[11] can be compared with the calculated phase diagram in equilibrium with iron shown in Fig. 7.

Yazawa and Kameda[28] presented the Cu_2S-FeO-FeS phase diagram at iron saturation. The extrapolation of their liquidus to the FeO-FeS section is given in Fig. 7.

Rosenqvist and Hartvig[23] equilibrated oxysulfide liquid with magnetite and the SO_2-S_2 gas flow with controlled $P(S_2)$ at a total pressure of 1 atm and 1135 or 1185 °C. Crucibles were made from alumina lined with magnetite. The liquid phase was analyzed for Fe, S and O by conventional methods: precipitation of iron as Fe_2O_3, electro-deposition of S as $BaSO_4$ and determination of the oxygen content by the hydrogen-reduction method (heating the sample in hydrogen to convert oxygen into water, which

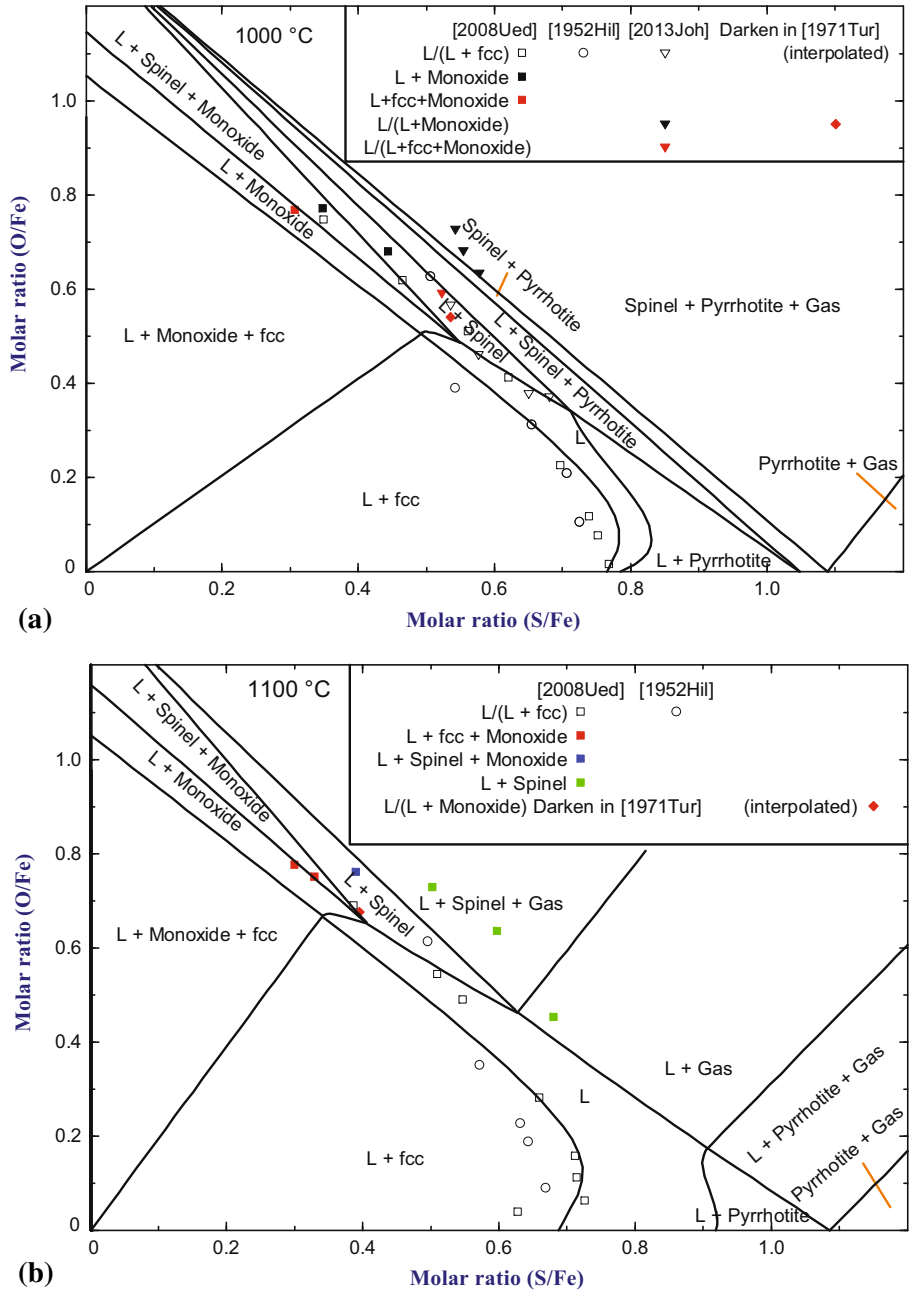

Fig. 6 Isothermal sections of the Fe-S-O phase diagram with superimposed O_2 and S_2 isobars at the total pressure of 1 atm and (a) 1000 °C, (b) 1100 °C, (c) 1120 °C, (d) 1200 °C, (e) 1300 °C, (f) 1400 °C and (g) 1450 °C. Experimental points are from Ref 21–24, 26, and 27. The solid lines are the calculated phase boundaries. The dotted and dashed lines in figures (c to e) are the calculated O_2 and S_2 isobars, respectively. The experimental tie-lines in figures (f and g) are shown by the dotted lines

was absorbed with P_2O_5). The compositions of the liquid phase in equilibrium with magnetite and SO_2-S_2 gas are plotted in Fig. 6(c,d).

Bog and Rosenqvist[24] prepared the H_2S-H_2O-H_2 gas mixtures of certain composition and equilibrated them with iron sulfide at 1120 °C, *i.e.* both $P(O_2)$ and $P(S_2)$ were fixed in these experiments. The crucible material was not reported. The composition of resulting melt was determined by unspecified chemical methods. Some experiments were conducted at iron saturation. The compositions of the samples in equilibrium with iron along with oxygen and sulfur isobars are plotted in Fig. 6(c).

Ueda et al.[27] melted mixtures of Fe, Fe_2O_3 and FeS in iron crucibles at 1000-1400 °C. The oxygen partial pressure was measured using the following oxygen concentration cell:

$$\text{Pt} \mid \text{Ni,NiO} \mid \text{ZrO}_2(\text{CaO}) \mid \text{specimen} \mid \text{Re} \mid \text{Pt} \qquad \text{(Eq 10)}$$

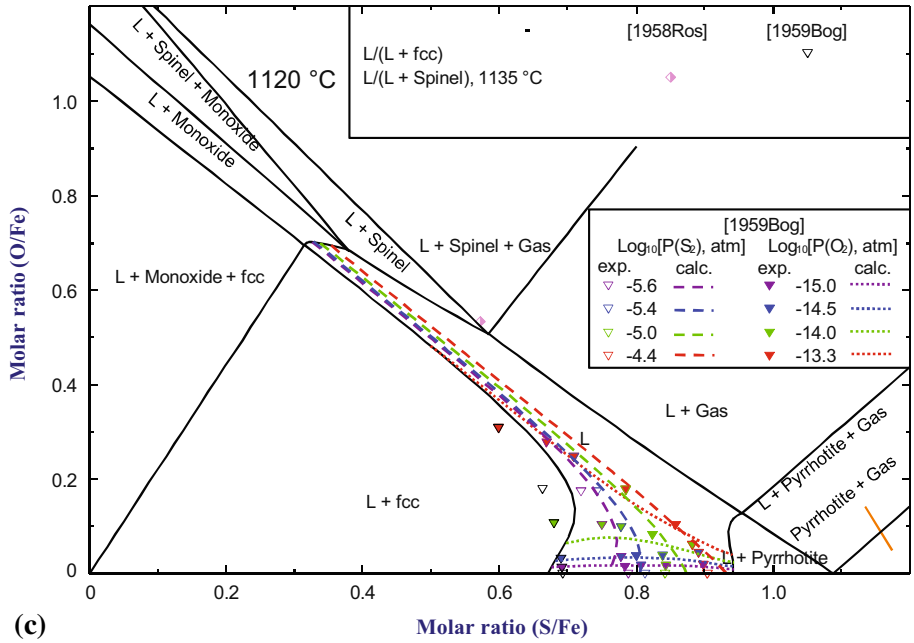

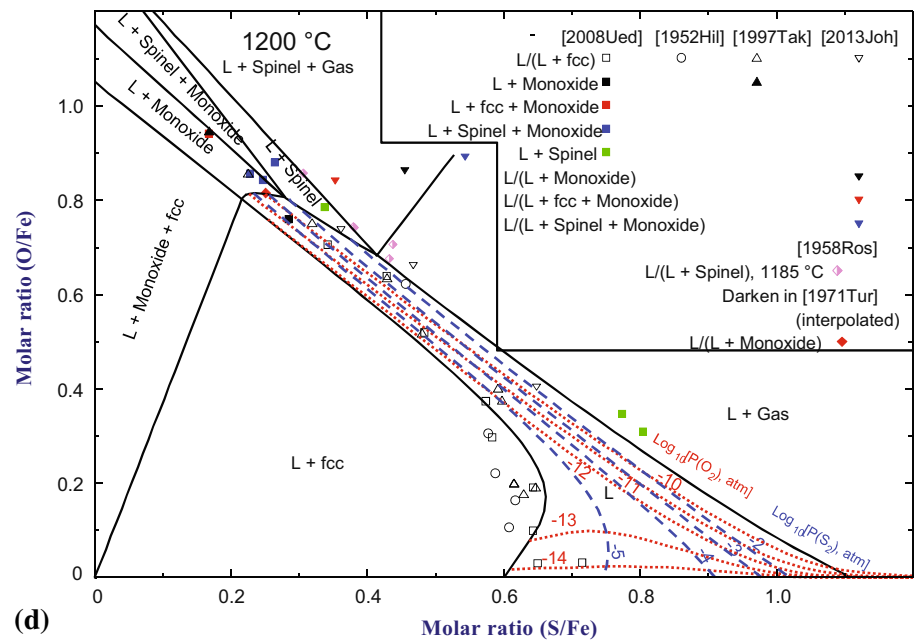

Fig. 6 continued

After equilibration, the crucible was quenched in a water bath. Compositions of the specimens were determined by chemical analysis. Oxygen and sulfur contents were determined by reduction with hydrogen. Iron was determined by titration methods and from the mass balance. The phase equilibrium results are shown in Fig. 6(a,b,d,e,f) and the oxygen potential measurements are given in the next Section in Fig. 8 and 9.

Takeda[26] melted the Fe-S-O mixtures in iron crucibles at 1200 and 1300 °C and measured the oxygen potential with a sensor similar to cell (10). The method used for chemical analysis was not reported. The results are shown in Fig. 6(d,e) and in the next Section in Fig. 9.

Johto et al.[12] heated mixtures of the pure Fe, FeS and Fe_2O_3 powders in crucibles lined with iron foil. The experiments were conducted either in an Ar atmosphere or at $P(O_2)$ controlled by the CO/CO_2 gas flow. After heat treatment, the samples were quenched. Microscopic observations showed that the Fe-"FeS"-"FeO"-L eutectic should be between 915 and 920 °C. The iron and sulfur contents of

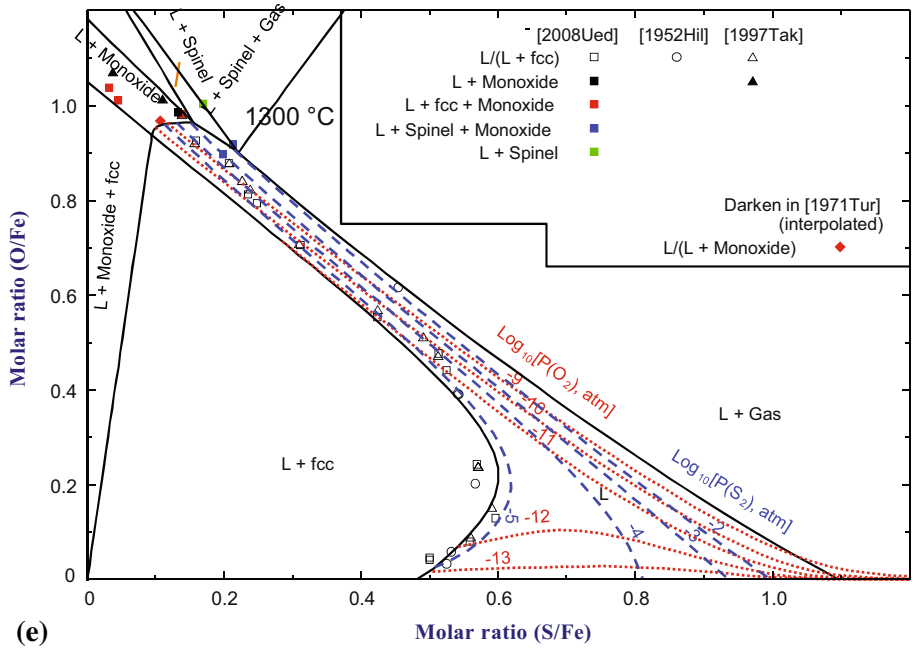

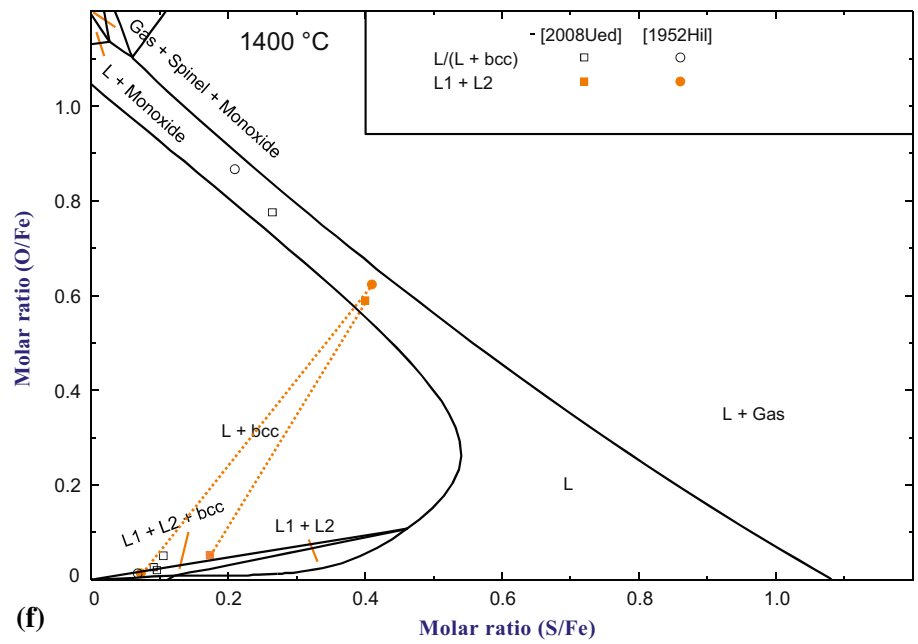

Fig. 6 continued

the liquid phase in equilibrium with solid phases were determined by EMPA analysis. The oxygen content was not measured directly and was obtained by difference, which makes the reported compositions relatively less accurate. The position of the eutectic point suggested by Johto et al.[12] is shown in Fig. 5 and 7. The compositions of the liquid phase in equilibrium with solids are plotted in Fig. 6(a, d). The dependence of the liquid composition on $P(O_2)$ is discussed in the next Section and plotted in Fig. 9.

Lee et al.[29] equilibrated mixtures of "FeO", FeS and Ag in iron crucibles under the flow of CO/CO_2. After equilibration, silver was analyzed for sulfur and "each component" of oxysulfide liquid was determined "by a gas analyzer and titration method". Since the results of analyses are not provided, it is not possible to evaluate the extent of contamination of the oxysulfide phase by silver. The measured compositions of oxysulfide liquid in equilibrium with iron were plotted by Lee et al.[29] in the Fe-S-O triangle. These compositions have much higher sulfur content than reported by Hilty and Crafts,[21] Ueda et al.,[27] Takeda[26] and even Johto et al.,[12] which may be due to the presence of silver in the liquid phase. Hence,

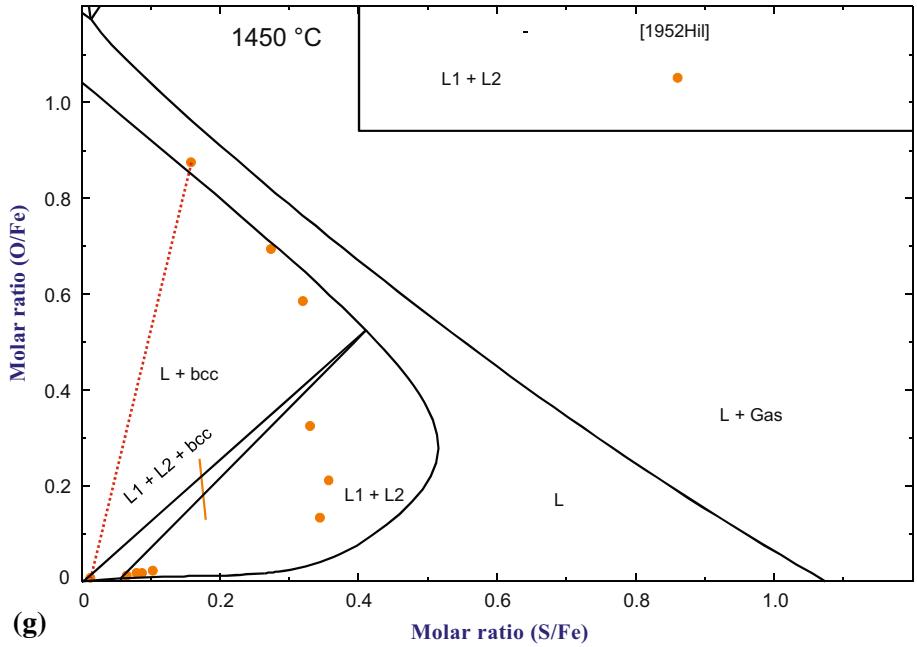

Fig. 6 continued

the results of Lee et al.[29] were not used in the present optimization.

As can be seen from Fig. 5 and 6, the phase relations in the Fe-S-O system are complex and somewhat unusual. The liquid phase substantially deviates from the FeO-FeS join both towards iron and nonmetals. It splits into two liquids at high temperatures. The miscibility gap becomes wider rather than narrower with an increase in temperature. The measured compositions are not very accurate, which is evident from the wide scatter of the experimental points corresponding to the L/(L + fcc) phase boundary shown in Fig. 6. The reported FeO-FeS phase diagram[11,22,28] was measured at iron saturation rather than by studying the compositions along the FeO-FeS section, which inevitably shifts the composition of the liquid phase from the FeO-FeS join (see Fig. 5). The calculated phase diagram at iron saturation is shown in Fig. 7.

5.2 Solubility of Oxygen and Sulfur in Oxysulfide Liquid

The solubility of oxygen and sulfur in oxysulfide liquid was measured by Bog and Rosenqvist,[24] Dewing and Richardson,[30] Nagamori and Kameda,[31] Kameda and Yazawa,[32] Stofko et al.,[33] Mintsis et al.,[34] Blatov et al.,[35] Nagamori and Yazawa,[36] Rose and Brenan,[37] Fonseca et al.,[38] Ueda et al.[27] and Johto and Henao.[12]

Dewing and Richardson[30] heated small samples of the condensed phase in a stream of N_2-S_2-SO_2. The melts were held in a platinum spiral. After attaining equilibrium, the samples were quenched and analyzed by treatment in hydrogen. The resulting H_2S was absorbed by the zinc acetate solution. Residual metal was dissolved in acid giving the iron content. Insoluble platinum was weighted. It was found that the quenched samples contained up to 2 mol% of platinum sulfide at high $P(S_2)$. Thus, iron, sulfur and platinum were determined directly and oxygen by difference. Most data points were obtained at 1206 °C. The partial pressures of S_2 and SO_2 were reported by the authors and equilibrium $P(O_2)$ was calculated in this study. The data are plotted in Fig. 8.

Nagamori and Kameda[31] equilibrated Fe-O-S melts with CO-CO_2-SO_2 gas mixtures at 1200 °C in alumina crucibles. The quenched samples were analyzed for the iron content by titration with $KMnO_4$, for sulfur by precipitation as $BaSO_4$, and for oxygen by the hydrogen reduction method. No initial gas compositions were reported by the authors, only calculated $P(S_2)$ and $P(O_2)$. The results are presented in Fig. 8.

Kameda and Yazawa[32] equilibrated Cu-Fe-O-S liquid with CO-CO_2-SO_2 gas mixtures at 1150 to 1225 °C in alumina crucibles. The copper, iron and sulfur contents were determined analytically and the oxygen content was measured by the hydrogen reduction method. Even though ten different CO/CO_2/SO_2 ratios were used, only the results for one gas composition were reported and used in the present study to calculate equilibrium $P(O_2)$ and $P(S_2)$. The copper-free point is plotted in Fig. 8.

Stofko et al.[33] studied Fe-S-O melts in equilibrium with N_2-S_2-SO_2 gas at 1200 °C in alumina crucibles. The quenched samples were analyzed for the iron content by titration with $KMnO_4$, for sulfur by precipitation as $BaSO_4$, and for oxygen by the hydrogen reduction method. No initial gas compositions were reported by the authors, instead, the calculated $P(S_2)$ and $P(O_2)$ were given. The data are plotted in Fig. 8.

Mintsis et al.[34] equilibrated Fe-O-S melts and CO-CO_2-SO_2 gas mixtures at 1200 and 1300 °C. The iron and sulfur contents in the quenched samples were obtained by

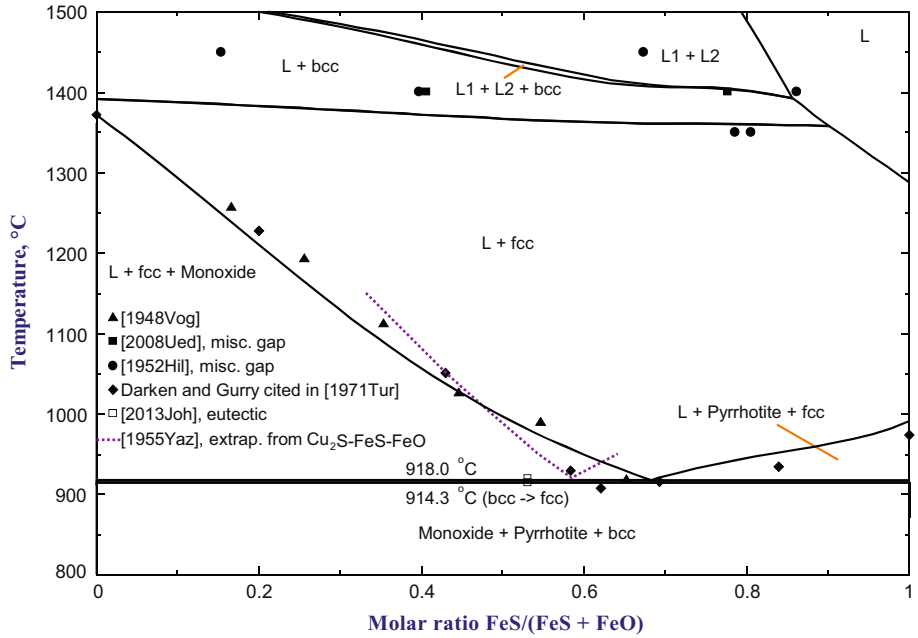

Fig. 7 Projection of the Fe-S-O phase diagram in equilibrium with iron on the FeS-FeO section through the Fe corner. Experimental points from Ref 12, 21, 22, 27, and 28

chemical analysis. The oxygen content was determined by difference in some samples and by an unspecified analytical method in controlled samples. The $CO/CO_2/SO_2$ ratios were reported and used in the present study to calculate $P(O_2)$ and $P(S_2)$. The results for 1200 °C are presented in Fig. 8.

Nagamori and Yazawa[36] equilibrated Fe-O-S melts with CO-CO_2-SO_2 gas mixtures at 1200 °C in alumina crucibles. The molten samples were quenched and analyzed for oxygen, sulfur and iron. Sulfur and iron were determined gravimetrically: sulfur as $BaSO_4$ and iron as Fe_2O_3. Oxygen was analyzed by the hydrogen reduction method. The analytical results and compositions of ingoing CO-CO_2-SO_2 gas were reported. The data are given in Fig. 8.

Fonseca et al.[38] equilibrated Fe-O-S melts with CO-CO_2-SO_2 gas mixtures at 1200 to 1400 °C in silica crucibles. Electron microprobe analysis (EMPA) was used to measure the contents of all elements, including oxygen, in the quenched samples. The $CO/CO_2/SO_2$ ratios were reported. The results for 1200 °C are presented in Fig. 8.

Blatov et al.[35] and Rose and Brenan[37] equilibrated Fe-O-S melts with CO-CO_2-SO_2 gas mixtures at 1300 °C. The crucible material and analytical methods were not reported in the former paper. In the latter work, San Carlos olivine mega crystal was used as a crucible and the samples were analyzed by EMPA, even for oxygen. The $CO/CO_2/SO_2$ ratios were reported in both studies.

From Fig. 8 it is evident that there are some discrepancies between the results of different authors at 1200 °C. Nagamori and Kameda[31] suggest lower sulfur contents and higher oxygen contents than Dewing and Richardson,[30] Kameda and Yazawa[32] and Stofko et al.[33] On the contrary, Fonseca et al.[38] give higher sulfur contents and lower oxygen contents compared to the same studies.[30,32,33] The data of Stofko et al.[33] are rather scattered, so that the dependence on $P(S_2)$ is mostly within the experimental scatter, while the results of Mintsis et al.[34] suggest that the solubility of sulfur is essentially independent of $P(S_2)$. The experimental data at higher temperatures[34,35,37,38] are even more scattered. The scatter is probably due to difficulties in attaining equilibrium between the liquid and gas phases when two partial pressures are fixed, especially at high $P(S_2)$.

The experimental results for the oxygen partial pressure over liquid saturated with solid iron[12,24,26,27] are summarized in Fig. 9. These data are much more reliable and consistent.

5.3 Solubility of Oxygen and Sulfur in Liquid Iron

The solubility of oxygen and sulfur in metallic liquid was measured by Hilty and Crafts,[21] Hayashi and Uno,[39] Schenck and Hinze.[40]

Hilty and Crafts[21] studied the equilibrium between Fe-rich liquid (liquid iron, L1) and FeO-rich liquid (slag, L2) in the Fe-S-O system using a rotating furnace at 1450 to 1650 °C. Samples were melted in magnesia crucibles under an Ar atmosphere. Slag was contaminated with MgO from the crucible material (up to 2.5 wt.%) and by SiO_2 from the thermocouple protection tube (up to 4 wt.%), though this is much less than the equilibrium solubility of MgO and SiO_2 in slag under the conditions of the experiments. Samples of liquid iron were analyzed: oxygen was determined by a variant of the vacuum-fusion method and sulfur was measured gravimetrically. The experimental results are plotted in Fig. 10.

Hayashi and Uno[39] equilibrated liquid iron with H_2S-H_2O-H_2-Ar mixtures at 1500 to 1600 °C in alumina crucibles. Oxygen and sulfur were analyzed by the vacuum

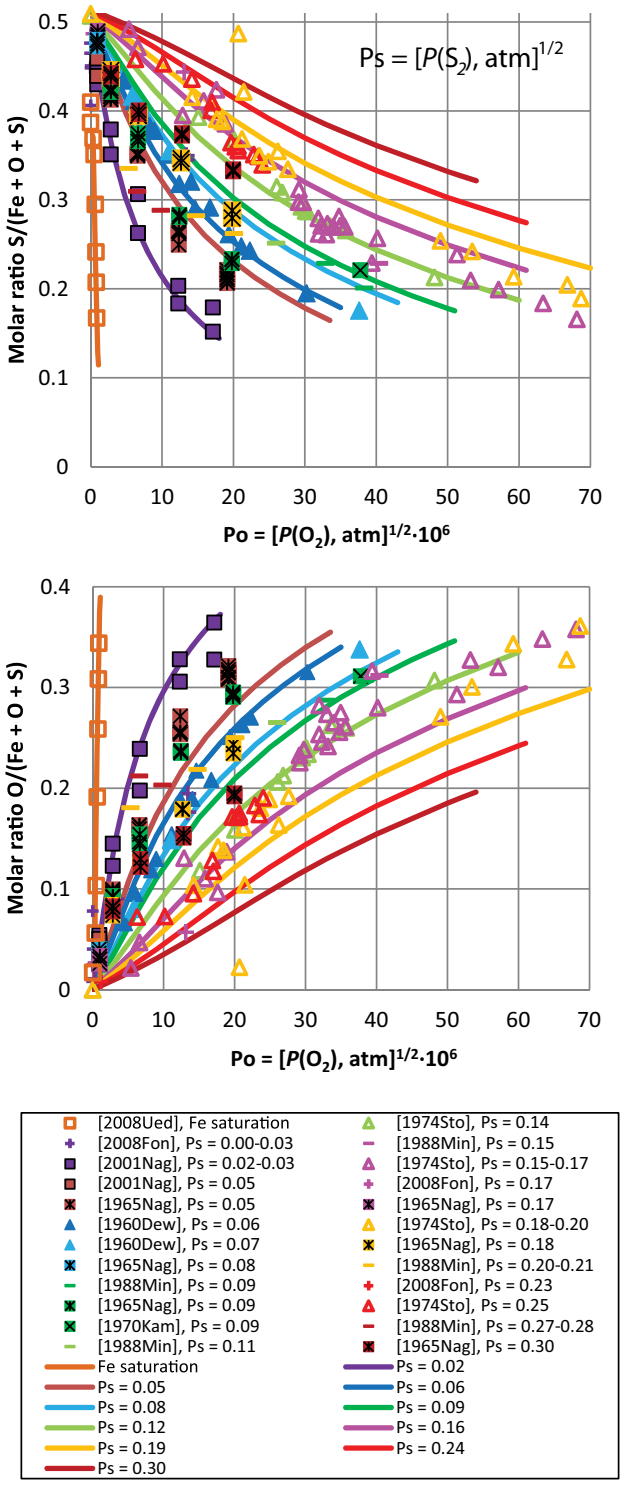

Fig. 8 Solubility of oxygen and sulfur in Fe-O-S oxysulfide melt at 1200 °C

fusion method. The obtained alloy compositions are shown in Fig. 10. The equilibrium $P(O_2)$ and $P(S_2)$ were calculated from the experimental gas compositions. The activity coefficient of oxygen defined as

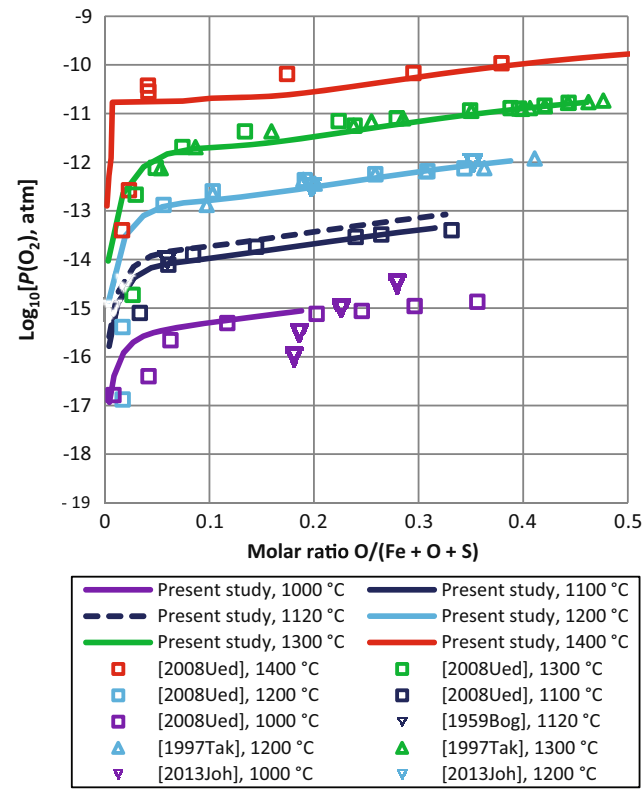

Fig. 9 Partial pressure of oxygen for oxysulfide liquid in equilibrium with iron in the Fe-O-S system: experimental points[12,24,26,27] and calculated lines. The kink and horizontal part of the calculated line at 1400 °C reflect the presence of the miscibility gap

$$\ln \gamma_O = 0.5 \ln P(O_2) - \ln X_O \quad \text{(Eq 11)}$$

is plotted in Fig. 11. The activity coefficient of sulfur was calculated in a similar way:

$$\ln \gamma_S = 0.5 \ln P(S_2) - \ln X_S \quad \text{(Eq 12)}$$

The results are shown in Fig. 12.

Schenck and Hinze[40] equilibrated liquid iron with CO/CO_2 gas of known composition in alumina crucibles at 1600 and 1650 °C. The quenched samples were analyzed for oxygen content by gas chromatography. No analysis for S after equilibration was reported, it was assumed that the initial S content from FeS did not change. The experiments were first made using sulfur-free samples, and then the effect of sulfur on the oxygen content was measured by addition of known amounts of FeS. The activity coefficient of oxygen in the liquid phase, f_O, was defined using weight rather than mole fractions as it is normally done in the technical literature[41]:

$$\mu_O = 0.5\mu^{+}_{O_2}(T) + RT \ln(f_O W_O) = 0.5[\mu^{+}_{O_2}(T) + RT \ln P(O_2)] \quad \text{(Eq 13)}$$

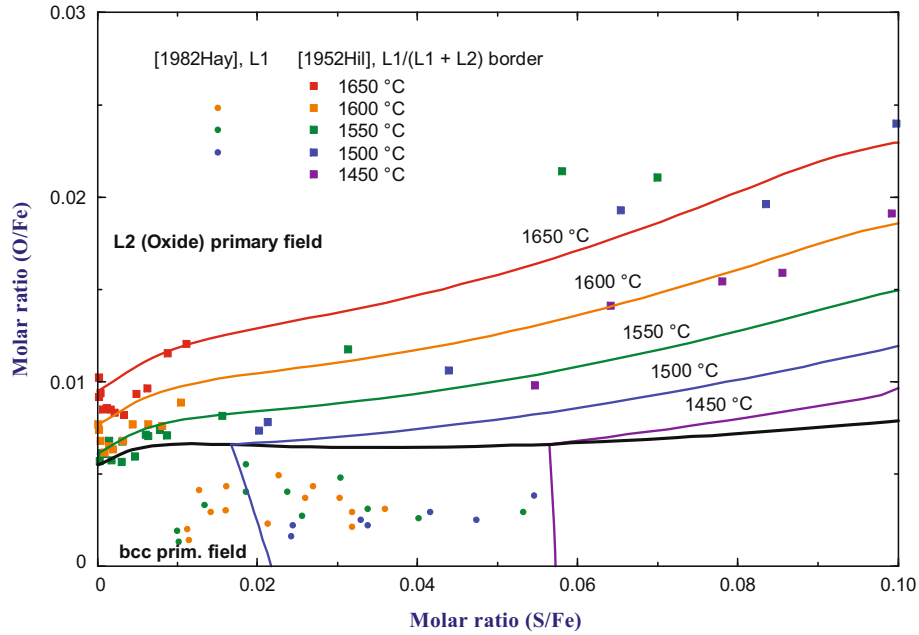

Fig. 10 Liquidus projection of the Fe-S-O system near the Fe corner. Experimental points[21,39] and calculated lines

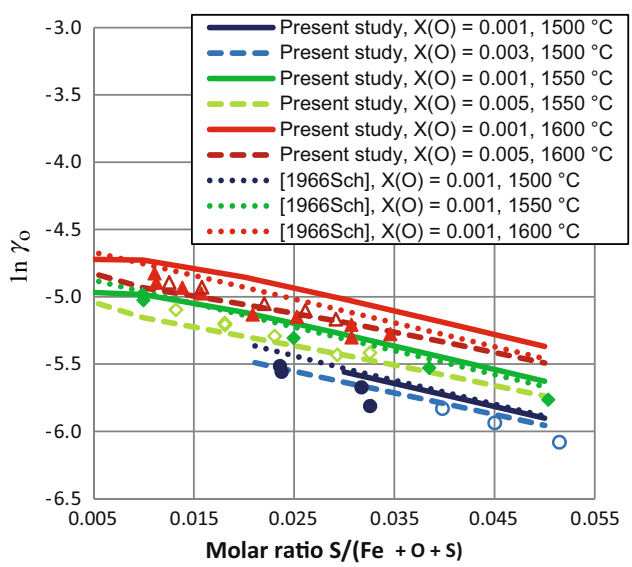

Fig. 11 Effect of sulfur on the activity coefficient of oxygen in Fe-O-S metallic liquid: experimental points[39] and calculated lines. The amounts of oxygen for the experimental points are approximately the same as for the calculated lines of the same color; the solid and open points correspond to the solid and dashed lines, respectively. The dotted lines were calculated using parameters of Eq 14 obtained by Schenck and Hinze[40]

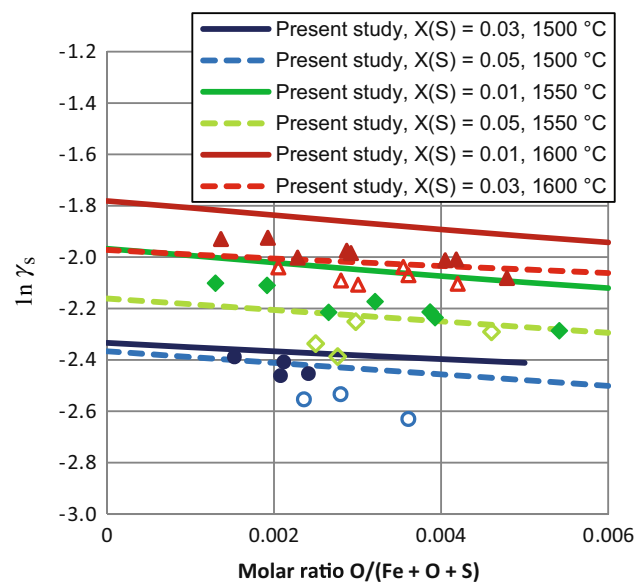

Fig. 12 Effect of oxygen on the activity coefficient of sulfur in Fe-O-S metallic liquid: experimental points[39] and calculated lines. The amounts of sulfur for the experimental points are approximately the same as for the calculated lines of the same color; the solid and open points correspond to the solid and dashed lines, respectively

where $\mu^{+}_{O_2}$ is the Gibbs energy of ideal O_2 gas at 1 atm, W_O is the weight fraction of oxygen and $P(O_2)$ is the equilibrium oxygen partial pressure in atm. The composition dependence of the activity coefficient was represented by the following equation

$$\log_{10}(f_O) = \log_{10}\left(f^{\circ}_{O}(T)\right) + e^{O}_{O}(T) \cdot \text{wt.\% O} + e^{S}_{O}(T) \cdot \text{wt.\% S} \quad \text{(Eq 14)}$$

and the first-order interaction coefficient e^{S}_{O} was obtained. This value was adopted by the Steelmaking data sourcebook.[41] The dashed lines in Fig. 11 were calculated using

Table 1 Optimized properties of stoichiometric compounds and model parameters for liquid and solid solutions in the Fe-O-S system (J mol^{-1})

Compounds	Temperature range (K) and reference	Molar Gibbs energy $g(T)$
Fe_2O_3 (hematite)	[5]	
S	[1]	
FeS (troilite), FeS_2 (pyrite) 'Fe_7S_8'(monoclinic pyrrhotite) Fe_9S_{10}, $Fe_{10}S_{11}$, $Fe_{11}S_{12}$	[2]	
$FeSO_4$	298-800	$-766593.6 + 1296.4616T - 192.5487T\ln T - 0.01160265T^2 + 3.62620\times10^{-6}T^3 - 2218465.7T^{-1} - 43771.4131\ \ln T$
	800-2000	$-995911.2 + 927.0702\ T - 150.7843T\ln\ T - 0.00571347\ T^2 + 3366120.1\ T^{-1}$
	>2000	$-1012032.9 + 1085.46319T - 171.9552\ T\ln T$
$Fe_2(SO_4)_3$	298-800	$-2162375.9 + 3389.5842T - 502.1294T\ln T - 0.03361654T^2 + 1.00286\times10^{-5}T^3 - 5753633.2T^{-1} - 113714.9841\ln T$
	800-2000	$-2536943.7 + 1911.1100T - 346.0460T\ln T - 0.01728174T^2 + 4786562.7T^{-1} - 61977.2609\ln T + 12668.5367T^{0.5}$
	>2000	$-2801987.7 + 2867.9861T - 452.6104T\ln T$
Solutions		
Liquid (metal, oxide, sulfide)	Modified quasichemical model: (Fe^{II}, Fe^{III}, O, S); Grouping: Fe^{II}, Fe^{III} in group 1 and O, S in group 2	
$Z^{Fe^{II}}_{Fe^{II}Fe^{II}} = Z^{Fe^{III}}_{Fe^{III}Fe^{III}} = Z^{S}_{SS} = Z^{O}_{OO} = Z^{Fe^{II}}_{Fe^{II}Fe^{III}} = Z^{Fe^{III}}_{Fe^{III}Fe^{II}} = Z^{O}_{OS} = Z^{S}_{SO} = 6,\ Z^{Fe^{II}}_{Fe^{II}S} = Z^{S}_{SFe^{II}} = 2,\ Z^{Fe^{II}}_{Fe^{II}O} = 2,\ Z^{O}_{OFe^{II}} = 2,\ Z^{S}_{SFe^{III}} = 3,\ Z^{Fe^{III}}_{Fe^{III}S} = 2,\ Z^{O}_{OFe^{III}} = 3,\ Z^{Fe^{III}}_{Fe^{III}O} = 2$		
g°_{O}	[1]	
$g^{\circ}_{Fe^{II}}$	298-1811[43]	$13265.9 + 117.5756T - 23.5143T\ln T - 0.00439752T^2 - 5.89269\times10^{-8}T^3 + 77358.5T^{-1} - 3.6751551\times10^{-21}T^7$
	1811-6000[43]	$-10838.8 + 291.3020T\text{-}46.0000T\ln T$
$g^{\circ}_{Fe^{III}}$	298-3500	$g^{\circ}_{Fe^{II}} + 6276.0$
g°_{S}	[1]	
$\Delta g^{\circ}_{Fe^{II}S}$	[2]	$-104888.10 + 0.3388T$
	This study	$-122334.14 + 112.4659T - 13.7582T\ln T$
$g^{01}_{Fe^{II}S}$, $g^{02}_{Fe^{II}S}$, $g^{03}_{Fe^{II}S}$, $g^{10}_{Fe^{II}S}$, $g^{20}_{Fe^{II}S}$, $g^{40}_{Fe^{II}S}$	[2]	
$\Delta g^{\circ}_{Fe^{II}O}$		-391580.56
$g^{10}_{Fe^{II}O}$		$129778.63 - 30.3340T$
$\Delta g^{\circ}_{Fe^{III}O}$		$-394551.20 + 12.5520T$
$g^{20}_{Fe^{III}O}$		83680.00
$q^{001}_{Fe^{II}Fe^{III}(O)}$	Bragg-Williams parameter	$30543.20 - 44.00414T$
$\Delta g^{\circ}_{Fe^{II}Fe^{III}}$		83680.00
$q^{102}_{SO(Fe^{II})}$	Bragg-Williams parameter	$292567.68 - 204.2804T$
$g^{001}_{Fe^{II}S(O)}$		$22044.34 - 17.80426T$
$g^{002}_{Fe^{II}S(O)}$		$27764.62 - 22.25532T$
$g^{101}_{Fe^{II}O(S)}$		-23012.00
$g^{901}_{Fe^{II}O(S)}$		$-41553.40 + 41.84000T$
$g^{002}_{Fe^{III}O(S)}$		-21756.80
fcc (Solid Fe)	Bragg-Williams (Fe, O, S)	
g°_{Fe}	298-1811[43]	$-236.5 + 132.4156T - 24.6643T\ln T - 0.003758T^2 + 77359.0T^{-1} - 5.8927\times10^{-8}T^3$
	1811-6000[43]	$-27097.2 + 300.2521T - 46.0000T\ln T - 2.78854\times10^{31}T^{-9}$
g°_{S}	[1]	
g°_{O}	[1]	
$L_{Fe,S}$		$-59070.74 - 34.61218T$
$L_{Fe,O}$		$-315652.63 - 27.61440T$

Table 1 continued

Compounds	Temperature range (K) and reference	Molar Gibbs energy $g(T)$
Magnetic properties of Fe	[44]	T_{Neel} = 67 K Magnetic moment β = 0.70 Structure-dependent parameter P = 0.28
bcc (Solid Fe)	Bragg-Williams (Fe, O, S)	
g°_{Fe}	298-1811[43]	$10375.2 + 114.5502T - 23.5143T\ln T - 0.004398T^2 + 77359.0T^{-1} - 5.8927\times10^{-8}T^3$
g°_{S}	298-368.3[2]	$19725.8 + 41.0945T - 11.0070T\ln T - 0.026529T^2 + 7.754333\times10^{-6}T^3$
	368.3-1300[2]	$18441.0 + 80.3697T - 17.9418T\ln T - 0.010895T^2 + 1.402558\times10^{-6}T^3 + 39910T^{-1}$
g°_{O}	Same as in fcc[1]	
$L_{Fe,S}$		$-29973.6 - 11.74268T$
$L_{Fe,O}$		$-315149.19 + 20.69349T$
Magnetic properties of Fe	[44]	T_{Curie} = 1043 K Magnetic moment β = 2.22 Structure-dependent parameter P = 0.40
Pyrrhotite ("$Fe_{1-x}S$")	[2]	
Wüstite ($Fe_{1-x}O$)	[5]	
Spinel (magnetite, $Fe_{3-x}O_4$)	[8,5]	

The thermodynamic properties of gaseous species were taken from the FactSage pure substance database[7]

Table 2 Calculated invariant points in the Fe-O-S system

Reaction upon cooling	T, °C	Composition of liquid (mole)			$\log_{10}[P(O_2)$, atm]	$\log_{10}[P(S_2)$, atm]	$\log_{10}[P(SO_2)$, atm]
		Fe	O	S			
L → Pyrrhotite + monoxide + fcc	918.0	0.50514	0.15711	0.33775	–16.39	–7.60	–8.14
L → Pyrrhotite + monoxide + Spinel	947.1	0.49418	0.18949	0.31634	–13.88	–5.15	–4.78
L (sulfur) + spinel → pyrrhotite + $FeSO_4$	982.0	0.00146	0.00001	0.99853	–7.82	1.79	4.31
L (metal) + L(oxysulfide) → L(oxysulfide) + bcc	1366.9	0.78269	0.00583	0.21148	–12.28	–4.76	–6.95

the parameters of Eq 14 from the Steelmaking data sourcebook,[41] assuming that e_O^S is independent of temperature.

5.4 Optimization

The database for the Fe-S system[2] was combined with the model parameters for the Fe-O system[5] to predict the thermodynamic properties and phase equilibria in the Fe-O-S system. The thermodynamic properties of stoichiometric $FeSO_4$ and $Fe_2(SO_4)_3$ were taken from the NIST-JANAF thermochemical tables.[42]

The phase relations in the Fe-O-S system predicted using only binary parameters for the liquid phase were qualitatively correct, but the agreement with the experimental data was not satisfactory quantitatively. Ternary parameters $g^{001}_{Fe^{II}S(O)}$ and $g^{002}_{Fe^{II}S(O)}$ were introduced to raise the monoxide liquidus and the eutectic temperature shown in Fig. 7. One more ternary parameter, $g^{101}_{Fe^{II}O(S)}$, and a Bragg-Williams parameter, $q^{102}_{SO(Fe^{II})}$, were required to suppress the low temperature immiscibility between liquid FeS_{1-x} and FeO and to increase the iron content in iron-saturated liquid (see Fig. 6). Another ternary parameter, $g^{002}_{Fe^{III}O(S)}$, was added to shift the phase boundary L/(L + Spinel + Gas) in Fig. 6(b) and (d) to higher S and O contents.

The binary parameter $\Delta g^{\circ}_{Fe^{II}S}$ was adjusted to raise γ_S in iron-rich Fe-S liquid at 1500 to 1600 °C in order to improve the description of the data of Hayashi and Uno[39] shown in Fig. 12. This did not impair the overall description of the experimental data in the Fe-S system. An additional parameter, $g^{901}_{Fe^{II}O(S)}$, was used to raise γ_O and γ_S in liquid iron (see Fig. 11, 12). However, the solubility of oxygen in liquid iron equilibrated with slag falls when γ_O increases, which made the description of the data of Hilty and Crafts[21] shown in Fig. 10 less accurate. A better fit of the data of Hayashi and Uno[39] and of Schenck and Hinze[40] would result in a large disagreement with the solubility data of Hilty and Crafts,[21] and also with the miscibility gap in Fig. 6(f,g) as reported by Hilty and Crafts[21] and Ueda et al.[27] And vice versa, if the miscibility gap between liquid iron and liquid oxysulfide were described more accurately, the activity coefficient of oxygen in Fig. 11 would fall dramatically. To resolve this contradiction, more experimental studies are required in the liquid iron region of the Fe-O-S system. In the present study, the model parameters were optimized to attain a reasonable compromise between the data on the activity coefficients of oxygen and sulfur in liquid iron[39,40] and the data on phase equilibria with oxysulfide liquid.[21,27]

The resulting description of the available experimental data is shown by the calculated lines in Fig. 3-12. In most cases the agreement is within the experimental error limits. However, the calculated miscibility gap L1 + L2 shown in Fig. 6(e, f) and 16 expands less rapidly with increasing temperature than suggested by the data of Hilty and Crafts[21] and Ueda et al.[27] The experimental L1 + L2 + bcc triangles at 1400 and 1450 °C are close to the calculated ones at 1470 and 1505 °C, respectively.

From the data on the solubility of oxygen and sulfur at fixed $P(O_2)$ and $P(S_2)$ summarized in Fig. 8, oxygen and sulfur isobars over the matte region can be calculated. In particular, these isobars at 1200 and 1300 °C are presented in Fig. 6(d, e).

The thermodynamic properties of all stoichiometric compounds and the values of the optimized model parameters are given in Table 1. The optimized parameters are strongly correlated and, therefore, are given in Table 1 with relatively large numbers of significant digits. The calculated invariant points are listed in Table 2.

6. Conclusions

A critical assessment and thermodynamic modeling have been performed for the Fe-O-S system over the whole composition range. A model for the liquid phase has been developed within the framework of the quasichemical formalism. This model describes simultaneously metallic liquid, sulfide liquid (matte) and oxide liquid (slag). For the Fe-O system, the model reflects the existence of two ranges of maximum SRO at approximately FeO and Fe_2O_3 compositions. Parameters of thermodynamic models for the liquid and solid phases have been optimized to provide the best description of all available thermodynamic and phase equilibrium data. The obtained self-consistent set of model parameters can be used to calculate the solubility of oxygen and sulfur in liquid and solid iron. The stability range of oxysulfide liquid can also be calculated at different temperatures along with the equilibrium oxygen and sulfur partial pressures at each composition.

The model parameters obtained in the present study are being used for development of a thermodynamic database for simulation of copper smelting and converting. In particular, the model and optimized properties of the liquid phase are essential for description of the solubility of oxygen in matte. The present study completes the optimization of all binary and ternary subsystems of the Cu-Fe-O-S quaternary system. The experimental data available for the Cu-Fe-O-S system were compared with the predictions from the combined database. Even though the agreement was fair, it was found that the Cu-Fe-S[2–4] optimization needs some improvement. Just a few additional model parameters that reflect interactions, which are present only in the quaternary system, may also be added to improve the description. The optimization of the Cu-Fe-O-S quaternary system will be reported elsewhere.

References

1. D. Shishin and S.A. Decterov, Critical Assessment and Thermodynamic Modeling of Cu-O and Cu-O-S Systems, *CALPHAD*, 2012, **38**, p 59-70
2. P. Waldner and A.D. Pelton, Thermodynamic Modeling of the Fe-S System, *J. Phase Equilib. Diff.*, 2005, **26**, p 23-28
3. P. Waldner, *Thermodynamic Modeling of the Cu-S System, Internal Report*, Ecole Polytechnique de Montreal, Montreal, QC, 2005

4. P. Waldner and A.D. Pelton, *Thermodynamic Modeling of the Cu-S System, Internal Report*, Ecole Polytechnioque de Montreal, Montreal, QC, 2006
5. T. Hidayat, D. Shishin, E. Jak, and S. Decterov, Thermodynamic Reevaluation of the Fe-O System, *Calphad*, 2015, **48**, p 131-144
6. D. Shishin, T. Hidayat, E. Jak, and S. Decterov, Critical Assessment and Thermodynamic Modeling of Cu-Fe-O System, *CALPHAD*, 2013, **41**, p 160-179
7. C.W. Bale, E. Belisle, P. Chartrand, S.A. Decterov, G. Eriksson, K. Hack, I.-H. Jung, Y.-B. Kang, J. Melancon, A.D. Pelton, C. Robelin, and S. Petersen, FactSage Thermochemical Software and Databases—Recent Developments, *CALPHAD*, 2009, **33**(2), p 295-311
8. S.A. Decterov, E. Jak, P.C. Hayes, and A.D. Pelton, Experimental Study and Thermodynamic Optimization of the Fe-Zn-O System, *Metall. Mater. Trans. B*, 2001, **32B**(4), p 643-657
9. A.D. Pelton, S.A. Decterov, G. Eriksson, C. Robelin, and Y. Dessureault, The Modified Quasichemical Model. I—Binary Solutions, *Metall. Mater. Trans. B*, 2000, **31B**(4), p 651-659
10. A.D. Pelton and P. Chartrand, The Modified Quasichemical Model. II—Multicomponent Solutions, *Metall. Mater. Trans. A*, 2001, **32A**(6), p 1355-1360
11. R. Vogel and W. Fulling: The System Iron-Iron Sulfide (FeS)-Wustite (FeO), *Festskr. J. Arvid Hedvall*, 1948, p 597-610
12. H. Johto, H.M. Henao, E. Jak, and P. Taskinen, Experimental Study on the Phase Diagram of the Fe-O-S System, *Metall. Mater. Trans. B*, 2013, **44**(6), p 1364-1370
13. D. Shishin, "Development of a thermodynamic database for copper smelting and converting", Ph. D. thesis, Ecole Polytechnique of Montreal, 2013
14. J.M. Skeaff and A.W. Espelund, Electromotive Force Method for the Determination of Sulfate-Oxide Equilibria Results for the Magnesium, Manganese, Iron, Nickel, Copper and Zinc Systems, *Can. Metall. Q.*, 1973, **12**(4), p 445-454
15. K.C. Hsieh and Y.A. Chang, A Solid-State Emf Study of Ternary Nickel-Sulfur-Oxygen, Iron-Sulfur-Oxygen, and Quaternary Iron-Nickel-Sulfur-Oxygen, *Metall. Trans. B*, 1986, **17B**(1), p 133-146
16. T. Rosenqvist and A. Hofseth, Phase Relations and Thermodynamics of the Copper-Iron-Sulfur-Oxygen System at 700-1000 °C, *Scand. J. Metall.*, 1980, **9**(3), p 129-138
17. O.A. Musbah and Y.A. Chang, A Solid-State EMF Study of the Fe-S-O and Co-S-O Ternary Systems, *Oxid. Met.*, 1988, **30**(5–6), p 329-342
18. S.C. Schaefer, *Electrochemical Determination of Gibbs Energies of Formation of Manganese Sulfide and Iron Sulfide(Fe0.9S), RI, 8486*, Albany Res. Cent. Bur. Mines, Albany, OR, 1980
19. A.W. Espelund and H. Jynge, The Zinc-Iron-Sulfur-Oxygen System Equilibriums Between Sphalerite or Wurtzite, Pyrrhotite, Spinel, Zinc Oxide and a Gas Phase, *Scand. J. Metall.*, 1977, **6**(6), p 256-262
20. T. Rosenqvist and P.H. Hynne, The Reaction Between Iron Sulfide and Sulfur Dioxide, *Tidsskr. Kjemi. Bergves. Metall.*, 1953, **13**, p 196-200
21. D.C. Hilty and W. Crafts, Liquidus Surface of the Iron-Sulfur-Oxygen System, *J. Metals*, 1952, **194**, p 1307-1312
22. E.T. Turkdogan, G.J.W. Kor, L.S. Darken, and R.W. Gurry, Sulfides and Oxides in Iron-Manganese Alloys. I. Phase Relations in Iron-Manganese-Sulfur-Oxygen System, *Metall. Trans.*, 1971, **2**(6), p 1561-1570
23. T. Rosenqvist and T. Hartvig, The Thermodynamics of Fe-Cu Mattes, and Their Equilibrium with Magnetite, *Norges Tek.-Naturvitenskapelige Forskiningsrud Met. Kom. Meddel*, 1958, **12**, p 21-52
24. S. Bog and T. Rosenqvist, *A Thermodynamic Study of Iron Sulphide-Iron Oxide Melts*. Nat. Phys. Lab. Symp. No. 9, NPL, Teddington, 1959
25. A.J. Naldrett, A Portion of the System Fe-S-O Between 900 and 1080 °C and Its Application to Sulfide Ore Magmas, *J. Petrol.*, 1969, **10**(2), p 171-201
26. Y. Takeda, Oxygen potential measurement of iron silicate slag-copper-matte system. *Proceedings of International Conference Molten Slags, Fluxes Salts '97, 5th*. Iron and Steel Society, Warrendale, PA, 1997
27. S. Ueda, K. Yamaguchi, and Y. Takeda, Phase Equilibrium and Activities of Fe-S-O Melts, *Mater. Trans.*, 2008, **49**(3), p 572-578
28. A. Yazawa and M. Kameda, Fundamental Studies on Copper Smelting. III. Partial Liquidus Diagram for Cu_2S-FeS-FeO System, *Technol. Rep. Tohoku Univ.*, 1955, **19**(2), p 239-250
29. Y.S. Lee, S.M. Jung, and D.J. Min, Thermodynamic Study on Phase Equilibria in the Liquid Fe-S-O System, *Steel Res.*, 2002, **73**(11), p 461-466
30. E.W. Dewing and F.D. Richardson, Thermodynamics of Mixtures of Ferrous Sulphide and Oxide, *J. Iron Steel Inst.*, 1960, **194**, p 446-450
31. M. Nagamori and M. Kameda, Equilibriums Between the Fe-S-O System Melts and CO-CO_2-SO_2 Gas Mixtures at 1200°, *Trans. Inst. Metals (Jpn.)*, 1965, **6**, p 21-30
32. M. Kameda and A. Yazawa: Effects of Partial Pressures of Oxygen and Sulfur on the Oxygen Content in Copper Matte. Studies in Met. (Commemoration for Prof. Matoba), Tohoku University, 1970
33. M. Stofko, J. Schmiedl, and T. Rosenqvist, Thermodynamics of Iron-Sulfur-Oxygen Melts at 1200 °C, *Scand. J. Metall.*, 1974, **3**(3), p 113-118
34. V.P. Mintsis, A.G. Ryabko, L.S. Tsemekhman, G.P. Grodinskii, and Y.V. Fisher, Equilibrium in the Iron-Sulfur-Oxygen System, *Izv. Akad. Nauk SSSR Met.*, 1988, **1**, p 28-32
35. I.A. Blatov, B.P. Burylev, L.S. Tsemekhman, and S.L. Litvinov, Thermodynamics of the Interaction of Components of the Fe-S-O System in Equilibrium with the CO-CO_2-SO_2 Gas Phase at 1300 °C, *Metally*, 1997, **6**, p 34-36
36. M. Nagamori and A. Yazawa, Thermodynamic Observations of the Molten FeS-FeO System and Its Vicinity at 1473 K, *Metall. Mater. Trans. B*, 2001, **32B**(5), p 831-837
37. L.A. Rose and J.M. Brenan, Wetting Properties of Fe-Ni-Co-Cu-O-S Melts Against Olivine: Implications for Sulfide Melt Mobility, *Econ. Geol.*, 2001, **96**(1), p 145-157
38. R.O.C. Fonseca, I.H. Campbell, H.S.C. O'Neill, and J.D. Fitzgerald, Oxygen Solubility and Speciation in Sulphide-Rich Mattes, *Geochim. Cosmochim. Acta*, 2008, **72**(11), p 2619-2635
39. S. Hayashi and T. Uno, Activities of Sulfur and Oxygen in Liquid Iron, *Tetsu to Hagane*, 1982, **68**(13), p 1728-1736
40. H. Schenck and H. Hinze, Equilibriums of the Iron-Carbon-Oxygen System in the Temperature and Concentration Range of Molten Steel and the Effect of Phosphorus, Manganese, and Sulfur, *Arch. Eisenhuettenwes.*, 1966, **37**(7), p 545-553
41. Steelmaking Data Sourcebook. *Japan Society for the Promotion of Science, 19th Comm. On Steelmaking, Gordon & Breach Science*, New York, NY, 1988, 312 pp
42. M. Chase, *NIST-JANAF Thermochemical Tables*, 4th ed., NIST, Gaithersburg, 1998
43. A.T. Dinsdale, SGTE Data for Pure Elements, *CALPHAD*, 1991, **15**, p 317-425
44. I. Ansara and Å. Jansson, *Assesment of the Copper-Iron System*, Materials Research Center, The Royal Institute of Technology, Stockholm, Sweden, 1993